The Astrophysical Journal, 681:1035–1045, 2008 July 10

AN INFRARED SURVEY OF BRIGHTEST CLUSTER GALAXIES. II. WHY ARE SOME BRIGHTEST CLUSTER GALAXIES FORMING STARS?

Christopher P. O'Dea, Stefi A. Baum, George Privon, and Jacob Noel-Storr
Department of Physics, Rochester Institute of Technology, 84 Lomb Memorial Drive, Rochester, NY 14623-5603;
odea@cis.rit.edu, baum@cis.rit.edu, gcp1035@cis.rit.edu, jake@cis.rit.edu

Alice C. Quillen, Nicholas Zufelt, and Jaehong Park
Department of Physics and Astronomy, University of Rochester, Rochester, NY 14627;
zufelt72@potsdam.edu, jaehong@pas.rochester.edu, aquillen@pas.rochester.edu

Alastair Edge
Institute for Computational Cosmology, Department of Physics, Durham University,
Durham DH1 3LE, UK; alastair.edge@durham.ac.uk

Helen Russell and Andrew C. Fabian
Institute of Astronomy, Madingley Road, Cambridge CB3 0HA, UK; hrr27@ast.cam.ac.uk, acf@ast.cam.ac.uk

Megan Donahue
Physics and Astronomy Department, Michigan State University,
East Lansing, MI 48824-2320; donahue@pa.msu.edu

Craig L. Sarazin
Department of Astronomy, University of Virginia, P.O. Box 400325,
Charlottesville, VA 22904-4325; cls7i@mail.astro.virginia.edu

Brian McNamara
Department of Physics and Astronomy, University of Waterloo, 200 University Avenue West,
Waterloo, ON N2L 3G1, Canada; mcnamara@uwaterloo.ca

Joel N. Bregman
Physics Department, University of Michigan, Ann Arbor, MI 48109; jbregman@umich.edu

and

Eiichi Egami
Steward Observatory, University of Arizona, 933 North Cherry Avenue,
Tucson, AZ 85721; eegami@as.arizona.edu
Received 2007 November 23; accepted 2008 March 11

ABSTRACT

Quillen et al. presented an imaging survey with the *Spitzer Space Telescope* of 62 brightest cluster galaxies with optical line emission located in the cores of X-ray-luminous clusters. They found that at least half of these sources have signs of excess IR emission. Here we discuss the nature of the IR emission and its implications for cool core clusters. The strength of the mid-IR excess emission correlates with the luminosity of the optical emission lines. Excluding the four systems dominated by an AGN, the excess mid-IR emission in the remaining brightest cluster galaxies is likely related to star formation. The mass of molecular gas (estimated from CO observations) is correlated with the IR luminosity as found for normal star-forming galaxies. The gas depletion timescale is about 1 Gyr. The physical extent of the IR excess is consistent with that of the optical emission-line nebulae. This supports the hypothesis that star formation occurs in molecular gas associated with the emission-line nebulae and with evidence that the emission-line nebulae are mainly powered by ongoing star formation. We find a correlation between mass deposition rates ($\dot{M}_X$) estimated from the X-ray emission and the star formation rates estimated from the IR luminosity. The star formation rates are 1/10 to 1/100 of the mass deposition rates, suggesting that the reheating of the intracluster medium is generally very effective in reducing the amount of mass cooling from the hot phase but not eliminating it completely.

Subject headings: cooling flows — galaxies: active — galaxies: clusters: general — galaxies: elliptical and lenticular, cD — infrared: galaxies — stars: formation

1. INTRODUCTION

The hot $T \sim 10^7$–10^8 K X-ray-emitting gas is currently thought to constitute the bulk of the baryonic mass in rich clusters of galaxies. An important aspect of the overall physics of the intracluster medium (ICM) concerns the central regions of clusters ($r \lesssim 10$–100 kpc), where the inferred ICM densities and pressures in some cases are sufficiently high that cooling to $T \lesssim 10^4$ K can occur on timescales shorter than the cluster lifetime (e.g., Cowie & Binney 1977; Fabian & Nulsen 1977; Edge et al. 1992). These "cooling core" clusters often exhibit intense optical emission-line nebulae associated with the centrally dominant (cD) galaxies at their centers, together with blue continuum excess emission, and the strength of these effects appears to correlate with the cooling rate or central pressure of the X-ray-emitting gas (Heckman 1981; Johnstone & Fabian 1987; Romanishin 1987; McNamara & O'Connell 1992, 1993; Crawford & Fabian 1992, 1993; Allen 1995).

The previous paradigm pictured the ICM as a relatively simple place where gas cooled and slumped in toward the center of the cluster in a cooling flow with mass accretion rates of hundreds of solar masses per year (e.g., Fabian 1994). However, X-ray spectroscopy with *XMM-Newton* and *Chandra* has failed to find evidence for gas at temperatures below about one-third of the cluster virial temperature (e.g., Kaastra et al. 2001; Tamura et al. 2001; Peterson et al. 2001, 2003; Peterson & Fabian 2006). The limits on the luminosity of the intermediate-temperature gas imply reductions in the inferred mass accretion rates by factors of 5–10. Recent theoretical models indicate that intracluster conduction, combined with an episodic heat source in the cluster core, such as an AGN or star formation, are candidates for explaining both the X-ray emission from cluster cores and the optical emission-line phenomena associated with the cores with these rapidly cooling spectra (e.g., Ruszkowski & Begelman 2002; Voigt et al. 2002; Fabian et al. 2002; Narayan & Medvedev 2001). One widely considered possibility is that an important source of heat in the ICM is bubbles driven by radio galaxies (e.g., Baum & O'Dea 1991; Tucker & David 1997; Soker et al. 2002; Böhringer et al. 2002; Kaiser & Binney 2003; Omma et al. 2004; Dunn et al. 2005; Dunn & Fabian 2006; Birzan et al. 2004; Rafferty et al. 2006), which halt the cooling of the gas. The ICM now appears to be a very dynamic place where heating and cooling processes vie for dominance and an uneasy balance is maintained. Since these same processes may operate during the process of galaxy formation, the centers of clusters of galaxies provide low-redshift laboratories for studying the critical processes involved in galaxy formation and supermassive black hole growth. At the present time, the main questions are (1) how much gas is cooling out of the ICM? (2) how much star formation is ongoing? and (3) what is the impact of the gas and star formation on the central brightest cluster galaxy (BCG)?

As little mass is needed to power the AGNs at the centers of bright cluster galaxies, the only way to remove cooled gas from the ICM is to form stars. Measurements of the star formation rate (SFR) in cluster galaxies can therefore provide constraints on the efficiency of cooling, the fraction of gas that cools, and the needed energy input to prevent the remainder of the gas from cooling. It is also possible that the ICM in cluster galaxies is not in a steady state or experiencing periods of enhanced cooling and star formation and periods of relative activity when cooling is prevented. Star formation and associated supernovae also provide a source of mechanical energy, although this is not sufficient to match the X-ray radiative energy losses (McNamara et al. 2006).

ISO observations detected the cluster Sérsic 159-03 (Hansen et al. 2000). Recent *Spitzer* observations have demonstrated that star formation is common in cooling core BCGs (Egami et al. 2006b; Donahue et al. 2007b; Quillen et al. 2008, hereafter Paper I). An IR excess is found in about half of the sample of 62 BCGs studied by Paper I. In this paper we discuss the results of Paper I. We examine correlations in the data and discuss the implications for star formation in BCGs and the balance of heating and cooling in the ICM. Specifically, we search for correlations between SFRs, radio, Hα, CO, and X-ray luminosities and mass deposition rates estimated from the X-ray observations. In this paper all luminosities have been corrected or computed to be consistent with a Hubble constant $H_0 = 70$ Mpc^{-1} km s^{-1} and a concordance cosmology ($\Omega_M = 0.3$ and flat).

2. COMPARISON DATA

The properties of the BCG sample are discussed by Paper I. Comparison data for the BCGs in our sample are listed in Table 1 of Paper I. When available, this table lists X-ray (primarily *ROSAT* 0.1–2.4 keV), radio (1.4 GHz), and Hα luminosities (from long-slit spectra and SDSS data) and [O III] λ5007/H$_\beta$ flux ratios. BCGs can host both star formation and an AGN. X-ray luminosities provide a constraint on the mass in and radiative losses from the hot ICM. The Hα recombination line is excited by emission from hot stars produced during formation or from an AGN. We note that emission lines are detected in ~10%–20% of typical optically selected BCGs, ~30%–40% of X-ray-selected BCGs, and almost 100% of BCGs in cooling core clusters (Donahue et al. 1992; Crawford et al. 1999; Best et al. 2007; Edwards et al. 2007). To discriminate between the presence of an AGN and star formation, we have sought a measure of the hardness of the radiation field through the [O III] λ5007/Hβ optical line ratio. Fluxes in the radio also provide a constraint on the properties of the AGN. Below we discuss SFRs estimated using IR luminosities derived from aperture photometry listed in Paper I, molecular gas masses estimated from CO observations, and mass deposition rates measured from X-ray observations. The statistical tests for correlations between the various quantities are given in Table 1.

TABLE 1
Spearman Rank Order Correlation Coefficients

Plot Name (1)	Figure Number (2)	Correlation Coefficient (3)	Two-sided Significance (4)
L_X vs. L_{IR}	2	0.63	5.0×10^{-5}
F_X vs. F_{IR}	...	0.14	0.40
L_X vs. 8/5.8	3	0.38	3×10^{-3}
$L_{1.4\,GHz}$ vs. L_{IR}	4	0.41	0.02
$F_{1.4\,GHz}$ vs. F_{IR}	...	−0.09	0.61
$L_{H\alpha}$ vs. L_{IR}	5	0.91	3.6×10^{-12}
$F_{H\alpha}$ vs. F_{IR}	...	0.65	1.1×10^{-4}
L(Hα) vs. L(24 μm)	...	0.84	2×10^{-15}
F(Hα) vs. F(24 μm)	6	0.67	4×10^{-8}
M(H$_2$) vs. L_{IR}	7	0.95	1.3×10^{-10}
F(CO) vs. F_{IR}	...	0.81	1.7×10^{-5}

Notes.—Col. (1): Correlation being tested. Col. (2): Figure that plots the data. Col. (3): Spearman rank order correlation coefficients. Col. (4): Two-sided significance of the correlation's deviation from zero. The most significant correlations are that between Hα and IR luminosity and that between molecular gas mass and IR luminosity. Most correlations are done on both fluxes and luminosities.

3. ESTIMATED STAR FORMATION RATES

If the IR luminosity is powered by star formation, we can use the IR luminosity to estimate an SFR (e.g., Bell 2003; Calzetti 2008). But first we need to consider whether some sources have a contribution to the IR from a type II AGN with an optically bright accretion disk. Paper I identified Z2089, A1068, and A2146 as likely to have an AGN contribution based on red 4.5/3.6 μm color, an unresolved nucleus seen in IRAC color maps, and a high [O III]/Hβ flux ratio. R0821+07 was flagged as possibly similar, as it has an unresolved nucleus in IRAC color maps and a high [O III]/Hβ. It also has a remarkably red 8.0/5.6 μm color similar to a Seyfert 2 with an embedded dusty AGN. In Figure 1 we plot the ratio of 4.5 and 3.6 μm fluxes to redshift (data from Paper I). The clear trend seen is as expected for a passive stellar population but with a few notable exceptions. The sources with strong [O III] (Z2089, A1068, and A2146) lie above the trend, as do A2055 and A2627, which show evidence for a BL Lac continuum in optical spectra (Crawford et al. 1999). The two galaxies

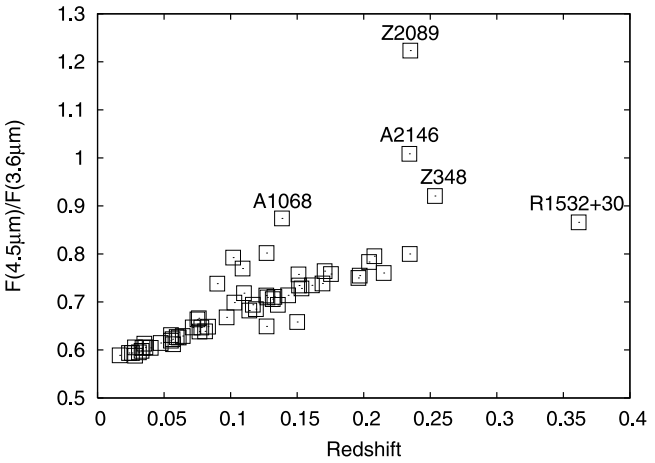

FIG. 1.—Flux ratio $F_{4.5\,\mu m}/F_{3.6\,\mu m}$ vs. redshift. The labeled objects show evidence for the presence of an optically luminous type II AGN.

that lie below the trend are Z2072 and Z9077 and are among the fainter objects in our sample. Z9077 was the only object not detected at 24 μm. The four that are between $z = 0.09$ and 0.15 and lie slightly above the trend are A1885, A2055, A2627, and R0352+19. It is not obvious why these four sources lie above the trend or whether this is significant. R0352+19 and R0821+07 are quite red in the 8.0/5.8 μm color, and R1532+30 and Z348 are pretty red in 8.0/5.8 μm but do not stand out in the 4.5/3.6 μm color versus z plot. Thus, the combination of diagnostics (4.5/3.6 μm color, red unresolved nuclear source, and high [O III]/Hβ ratio) identifies some sources with a strong AGN contribution. The remaining objects are likely to be free of strong AGN contamination.

Previous optical and UV observations have found evidence for significant star formation in the BCGs in cool core clusters (Johnstone & Fabian 1987; Romanishin 1987; McNamara & O'Connell 1989, 1993; McNamara 2004; McNamara et al. 2004; Hu 1992; Crawford & Fabian 1993; Hansen et al. 1995; Allen 1995; Smith et al. 1997; Cardiel et al. 1998; Hutchings & Balogh 2000; Oegerle et al. 2001; Mittaz et al. 2001; O'Dea et al. 2004; Hicks & Mushotzky 2005; Rafferty et al. 2006). Table 1 of Paper I lists [O III]/Hβ ratios for most of the BCGs. Except for the few which may host an AGN, the ratios are consistent with the gas being ionized by hot stars.

In Table 2 we present the estimated IR luminosities from Paper I and the estimated SFRs. The SFR can be estimated from the IR luminosity with equation (5) of Bell (2003),

$$\psi(M_\odot\ \mathrm{yr}^{-1}) = A\left(\frac{L_{\rm IR}}{L_\odot}\right)\left(1 + \sqrt{10^9\ L_\odot/L_{\rm IR}}\right). \qquad (1)$$

Here the constant $A = 1.57 \times 10^{-10}$ for $L_{\rm IR} > 10^{11}\ L_\odot$ and $A = 1.17 \times 10^{-10}$ at lower luminosities. The SFRs are in the range of about 1 to a few tens of $M_\odot$ yr^{-1}. The objects with SFRs above about 50 $M_\odot$ yr^{-1} are likely AGN-dominated.

In Table 3 we list available SFRs in different wave bands. We see that there is dispersion in the estimated SFRs. However, because of the effects of dust and geometry we do not necessarily expect agreement between SFRs estimated in the IR versus the UV/optical. Much of the variation can be accounted for by aperture mismatch; differences in assumptions about star formation history, i.e., burst versus constant star formation; extinction; and perhaps differences in the amount of dust available to reradiate in the far-IR (FIR). Note that A1068 and A2146 show large discrepancies between our FIR SFR and the U-band SFR, and both are flagged as possible AGNs. Given the expected dispersion, the rough agreement between the SFRs is consistent with the IR emission being dominated by star formation.

TABLE 2
STAR FORMATION RATE

Cluster	$L_{\rm IR}$ (10^{44} erg s^{-1})	SFR ($M_\odot$ yr^{-1})
Z2089*	64.68	271
A2146*	45.46	192
A1068*	44.61	188
R0821+07*	8.47	37
R1532+30*	22.62	97
Z8193*	13.70	59
Z0348*	11.92	52
A0011*	7.97	35
PKS 0745−1	3.80	17.2
A1664	3.21	14.6
R0352+19	2.40	11.1
NGC 4104	0.80	4.0
R0338+09	0.39	2.1
R0439+05*	4.17	18.7
A2204	3.23	14.7
A2627	1.59	7.5
A0115	1.30	6.2
Z8197	0.72	3.6
R2129+00	2.93	13.4
A1204	1.73	8.1
A0646	1.49	7.1
A2055	1.46	7.0
A0291	1.30	6.3
A1885	1.04	5.1
A3112	0.84	4.2
A2292	0.80	4.0
A1930	0.75	3.8
Z8276	0.74	3.7
A4095	0.29	1.6
A0085	0.28	1.6
A2052	0.24	1.4
R0000+08	0.20	1.2
NGC 6338	0.18	1.0
R0751+50	0.10	0.65
A0262	0.08	0.54

NOTES.—IR luminosities are from Paper I, estimated from the 15 μm wavelength for BCGs that are detected at 70 μm or have color ratios $F_{8\,\mu m}/F_{5.8\,\mu m} > 1.0$ or $F_{24\,\mu m}/F_{8\,\mu m} > 1.0$. The SFR was estimated using eq. (1). The top section contains four BCGs that are suspected to harbor dusty type II AGNs. Z2089, A2146, and A1068 exhibit a red $F_{4.5\,\mu m}/F_{3.6\,\mu m}$ color, and all four exhibit high [O III] λ5007/Hβ flux ratios. Note that if there is an AGN present in one of these clusters, the SFR may be overestimated. The second section contains the remaining nine BCGs with $F_{8\,\mu m}/F_{5.8\,\mu m} > 1.3$. The third section contains the set of five clusters with $1.0 < F_{8\,\mu m}/F_{5.8\,\mu m} < 1.3$. The fourth section contains the remaining BCGs with IR excesses. Specifically, they have ratios $F_{8\,\mu m}/F_{5.8\,\mu m} > 1.0$, $F_{24\,\mu m}/F_{8.0\,\mu m} > 1.0$, or a detected 70 μm flux. The BCGs marked with an asterisk can be classified as LIRGs since they have $L_{\rm IR}$ greater than $10^{11}\ L_\odot$. Objects with $F_{8\,\mu m}/F_{5.8\,\mu m} < 1.0$ or $F_{24\,\mu m}/F_{8\,\mu m} < 1$ and lacking a 70 μm detection are listed in Table 3 of Paper I with upper limits on $L_{\rm IR}$. For these objects $L_{\rm IR} \lesssim 0.3 \times 10^{44}$ erg s^{-1}, and corresponding SFRs are lower than $\lesssim 1\ M_\odot$ yr^{-1}.

3.1. *Caveat: The Dust-to-Gas Ratio*

The derived SFR might be underestimated if the cold gas in the BCGs has a low dust-to-gas ratio. This might be the case if the gas has cooled from the hot ICM and if the dust was destroyed while

TABLE 3
Comparison of Estimates of Star Formation Rate

BCG (1)	OD08 (2)	C99 (3)	HM05 (4)	MO93 (5)	M95 (6)	M04 (7)	M05 (8)	B03 (9)	MO89 (10)	OD04 (11)	D07 (12)
A262	0.5			0.02							
A2597				12						10	4
A1795		2	9	12					1.8	10	
A1835		77–125	123				100				
A1835							138 (FIR)				
Hydra A			9.5		1 (b)						
Hydra A					23–35 (c)						
A2052	1.4	0.96						0.4–0.6	0.16		
A1068	188	30				16–40					
A1068						68 (IR)					
A1664	14	23									
R1532	97	12									
A2146	192	5.6									
PKS 0745	17		129								

Notes.—Comparison of SFRs from this paper (col. [2]) with estimates from the literature (cols. [3]–[12]). Values are in units of $M_{\odot}$ yr^{-1}. References are as follows: OD08, this paper; C99, Crawford et al. (1999); HM05, Hicks & Mushotzky (2005); MO93, McNamara & O'Connell (1993); M95, McNamara (1995); M04, McNamara et al. (2004); M05, McNamara et al. (2006); B03, Blanton et al. (2003); MO89, McNamara & O'Connell (1989); OD04, O'Dea et al. (2004); D07, Donahue et al. (2007b). For Hydra A, (b) and (c) refer to "short-duration burst" and "continuous star formation models," respectively.

in the hot phase and there has not been sufficient time to form dust at the levels typically seen in normal star-forming galaxies. However, there are several arguments against a low gas-to-dust ratio: (1) The observations of H_2 (e.g., Donahue et al. 2000; Edge et al. 2002; Hatch et al. 2005; Jaffe et al. 2005; Egami et al. 2006a; Johnstone et al. 2007) and CO (Edge 2001; Salomé & Combes 2003, 2004) associated with the BCG optical emission-line nebulae require the presence of significant amounts of dust to shield the molecular gas. (2) Dust is clearly seen in the optical emission-line nebulae in cool core clusters (e.g., Sparks et al. 1989, 1993; McNamara & O'Connell 1992; Donahue & Voit 1993; Koekemoer et al. 1999). (3) Studies of the nebulae in the BCGs of cool core clusters suggest the presence of dust-to-gas ratios consistent with Galactic values (Sparks et al. 1989, 1993; Donahue & Voit 1993). (4) Theoretical arguments suggest that dust could form quickly inside cool clouds (Fabian et al. 1994; Voit & Donahue 1995).

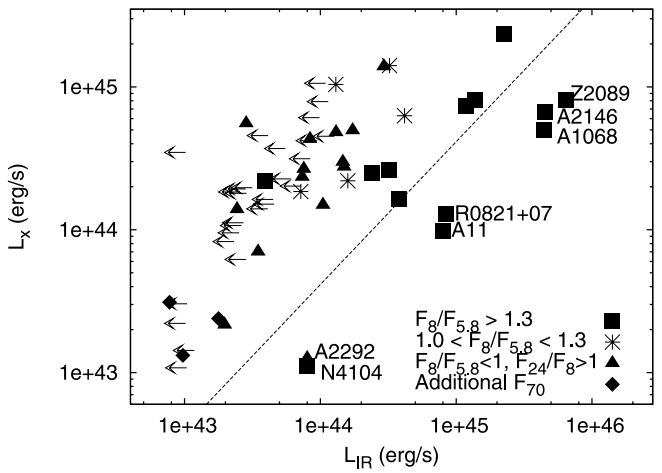

Fig. 2.—X-ray luminosity vs. estimated IR luminosity. X-ray and IR luminosities are listed in Tables 1 and 3 of Paper I. Squares represent our reddest group, with 8 μm–to–5.8 μm flux ratios greater than 1.3. The intermediate group, with flux ratios between 1.0 and 1.3, are plotted as asterisks. Triangles have 8 μm–to–5.8 μm flux ratios less than 1 but 24 μm–to–8 μm flux ratios above 1. Diamonds represent galaxies with both 24 μm–to–8 μm and 8 μm–to–5.8 μm flux ratios less than 1 but have been detected at 70 μm. Flux ratios are computed using photometry listed in Table 2 in Paper I. Upper limits on the IR luminosity are shown by arrows. We find a weak correlation between X-ray and IR luminosity. The dashed line shows the kinetic energy injection rate predicted from a star-forming population due to supernovae as a function of the IR luminosity. We confirm that kinetic energy from supernovae cannot account for the X-ray radiative energy losses in most cooling flows.

4. COMPARISON BETWEEN IR LUMINOSITY AND X-RAY LUMINOSITY

The integrated X-ray luminosity of a cluster is dependent on the combination of its core and larger scale structure. As such, any correlation between this global property and the properties of the BCG may indicate an underlying link, particularly as our sample from its selection will favor cool cores. Therefore, we plot the X-ray luminosity of the host cluster (listed in Table 1 of Paper I) against estimated IR luminosities for all BCGs with color ratio $F_{8\,\mu m}/F_{5.8\,\mu m} > 0.75$ in Figure 2. In Figure 3 we show X-ray luminosities compared to the color $F_{8\,\mu m}/F_{5.8\,\mu m}$. This study covers a much larger range in X-ray luminosity than Egami et al.

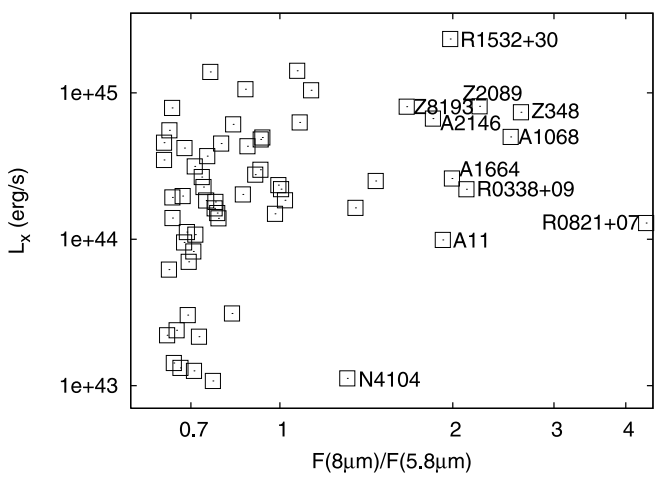

Fig. 3.—X-ray luminosity vs. 8 μm–to–5.8 μm flux ratio (data taken from Tables 1 and 2 in Paper I). Most red objects with $F_{8\,\mu m}/F_{5.8\,\mu m} > 1$ have X-ray luminosity $L_X > 10^{44}$ erg s^{-1}.

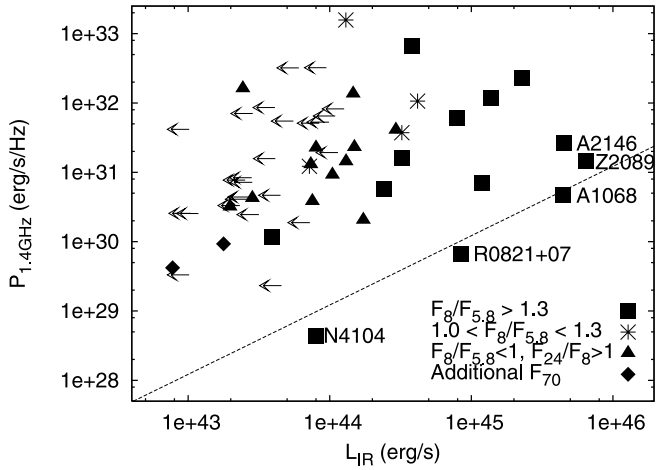

FIG. 4.—Radio luminosity at 1.4 GHz (listed in Table 1 of Paper I) vs. estimated IR luminosity (Table 2). The radio-IR correlation (eq. [2]) for star-forming objects is shown as a dashed line. The radio fluxes are much higher than expected from the radio-IR correlation appropriate for star-forming late-type galaxies. This is not unexpected, since many of these objects contain radio cores and in some cases even double-lobed jets. We find a weak correlation between the radio luminosity at 1.4 GHz and the IR luminosity. The symbols are the same as in Fig. 2.

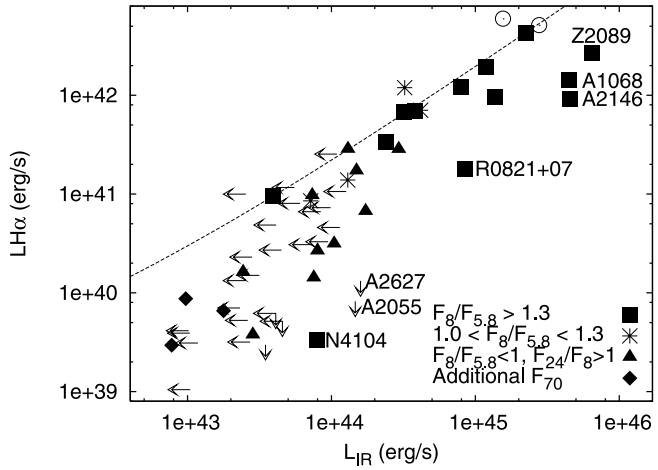

FIG. 5.—Observed Hα luminosity (listed in Table 1 of Paper I) vs. infrared luminosity estimated from the 8 and 24 μm fluxes. The data for two BCGs from Egami et al. (2006a) are shown as open circles. The Kennicutt relation inferred from observations of star-forming galaxies relating Hα luminosity to SFR is plotted as a dotted line. We have divided the line by a factor of 2.8 to remove the reddening correction, since our Hα luminosities are uncorrected for reddening. The Hα fluxes are consistent with the estimated IR luminosities and star formation. As in Fig. 2, the symbols depend on the 8 μm–to–5.8 μm color. We suspect that some of the Hα luminosities are lower than expected because the apertures used to measure them were smaller than those used to measure the IR fluxes.

(2006b). We see that BCGs with higher IR luminosity and redder 8 μm–to–5.8 μm colors (indicating an IR excess) tend to have higher X-ray luminosities. However, there are many objects with high X-ray luminosity ($L_X > 10^{44}$ erg s^{-1}) that do not have an IR excess.

It is interesting to compare the kinetic energy injected by supernovae (from an SFR consistent with the IR luminosity) to the energy radiated in X-rays. Leitherer et al. (1999) estimate a mechanical energy of about 10^{42} erg s^{-1} normalized for an SFR of 1 $M_\odot$ yr^{-1}. These conversion factors have been used to estimate the mechanical energy due to supernovae as a function of IR luminosity. This relation is shown in Figure 2 (*dashed line*). We see that there are a few BCGs for which there may be sufficient mechanical energy to resupply the X-ray luminosity. However, in general, for the sample as a whole, we confirm the finding of previous studies (e.g., McNamara et al. 2006) that mechanical energy input from supernovae is not sufficient (by a few orders of magnitude) to account for the current radiative energy losses of the ICM as a whole or in the core.

5. COMPARISON TO RADIO LUMINOSITY

We find a modest (almost 3 σ) correlation between the IR luminosity and the radio luminosity at 1.4 GHz (as we show in Fig. 4). We compare the radio fluxes to those appropriate for star-forming objects with a dashed line in the lower right portion of Figure 4. The radio-IR relation for star-forming objects (eq. [3] of Bell 2003) is

$$\left(\frac{L_{1.4\ \mathrm{GHz}}}{\mathrm{erg\ cm^{-2}\ s^{-1}\ Hz^{-1}}}\right) = \left(\frac{L_{\mathrm{IR}}}{3.75\times10^{12+q}\ \mathrm{erg\ cm^{-2}\ s^{-1}\ Hz^{-1}}}\right), \quad (2)$$

where q is a logarithmic index. We have used the mean value $q = 2.34$ by Yun et al. (2001).

In Figure 4 the majority of radio fluxes are well above this relation. The three objects below the line are (*left to right*) NGC 4104, R0821+07, and A1068. NGC 4104 is nearer than the other objects in the survey, and it is possible that the Hα flux and radio flux density have been underestimated. The other two clusters (A1068 and R0821+07) have $F_{8\ \mu m}/F_{5.8\ \mu m} > 1.3$ and have unresolved red sources seen in the IRAC color maps and so are likely to be dominated by an AGN.

Thus, the BCGs (independent of whether they have an IR excess) tend to have radio emission which is dominated by that produced by an AGN. Based on hot IR colors and high [O III]/Hβ ratios it appears that only four of the BCGs host a type II AGN with a luminous accretion disk (Paper I). Thus, either the AGNs in most of the BCGs are currently turned off, or they are accreting in a low-luminosity mode. The (weak) correlation between radio and IR luminosity may be a consequence of the correlation between mass accretion rate and SFR (§ 8); i.e., the cooling gas feeds the AGN and makes gas available for star formation. In addition, the ratio of mechanical energy in the radio source outflow to the radio luminosity can vary by about 3 orders of magnitude (Birzan et al. 2004). Thus, the radio luminosity can be a poor measure of the impact of the radio source on its environment.

6. COMPARISON TO Hα LUMINOSITY

We compare the Hα luminosities from limited-aperture spectroscopy to the IR luminosities in Figure 5, finding a strong correlation between the two. We also see a correlation in Hα flux versus 24 μm flux density (Fig. 6). These correlations show that the Hα and IR emission arises from the same or a related power source. We suggest that the dominant power source for the Hα and IR emission is star formation. This is consistent with previous evidence that the optical emission-line nebulae are mostly powered by UV photons from young stars with a possible secondary contribution from another mechanism (e.g., Johnstone & Fabian 1988; Allen 1995; Voit & Donahue 1997; Crawford et al. 1999; O'Dea et al. 2004; Wilman et al. 2006; Hatch et al. 2007). The Hα-SFR law relating the SFR to the Hα luminosity,

$$\mathrm{SFR}\left(M_\odot\ \mathrm{yr^{-1}}\right) = \frac{L(\mathrm{H}\alpha)}{1.26\times10^{41}\ \mathrm{erg\ s^{-1}}} \quad (3)$$

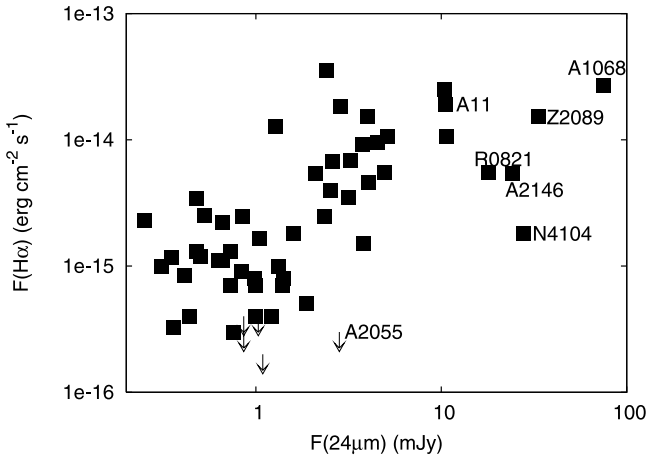

FIG. 6.—Observed Hα flux vs. 24 μm flux listed in Paper I. Arrows denote upper limits.

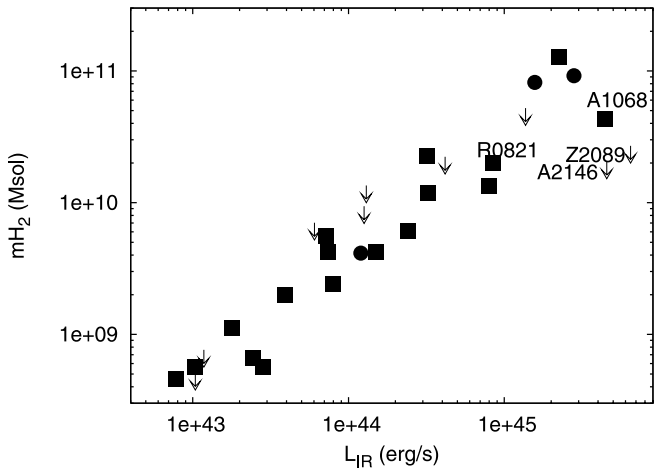

FIG. 7.—Correlation of H_2 mass from CO luminosity and L_{IR}. A1835 and Z3146, discussed by Egami et al. (2006a), and A2597, discussed by Donahue et al. (2007a), are shown as circles. We find a strong correlation and as such consider the relation between CO and star formation. Upper limits are shown as arrows. The four objects thought to host AGNs are labeled. Two of these have IR luminosities higher than expected from their molecular gas mass.

(Kennicutt 1998), is shown as a dashed line in Figure 5. We have scaled the line down by a factor of 2.8 because our Hα luminosities are uncorrected for reddening. We see in Figure 5 that the points tend to lie a factor of a few below this line; i.e., the observed luminosity in Hα is lower than that expected from the estimated IR luminosity. The discrepancy is larger at lower X-ray luminosity, $L_X < 10^{44}$ erg s^{-1}. Our Hα luminosities are taken mainly from spectroscopy with a long slit of width 1.3″ (Crawford et al. 1999) or the 3″ diameter fibers of the SDSS. Narrowband Hα+[N II] images and integral field unit observations give angular sizes for 11 of our BCGs and calibrated Hα+[N II] fluxes for 6 sources (Heckman 1981; Heckman et al. 1989; Cowie et al. 1983; Baum et al. 1988; McNamara et al. 2004; Wilman et al. 2006; Donahue et al. 2007a; Hatch et al. 2007). We find that the nebulae are all larger than the spectroscopic apertures, with a median size of 7.1″ (geometric mean of major and minor axes). The total fluxes determined from the narrowband images and IFU spectroscopy are larger than those from Crawford et al. (1999) or SDSS, with a median ratio of 1.4. Thus, it seems likely that aperture effects contribute to the Hα deficit, although larger samples with narrowband imaging are needed to determine whether this can explain the whole effect. In addition, strong absorption of Hα (relative to normal star-forming galaxies) could also contribute to the Hα deficit. However, the possibility remains that star formation is not the only power source for the Hα and IR emission. If this turns out to be the case, it would suggest that there is an additional source of energy which heats the dust but does not ionize the gas. Such an energy source would help to explain the observed optical line ratios (Voit & Donahue 1997) and bright H_2 emission (Edge et al. 2002; Jaffe et al. 2001, 2005).

7. COMPARISON TO MOLECULAR GAS MASS

We have compiled molecular mass data from Edge (2001), Salomé & Combes (2003), and A. C. Edge, in preparation. This subsample consists only of objects that have been surveyed for and detected in CO (1–0). The inferred molecular gas masses range from $\sim 10^9$ to $\sim 10^{11}$ $M_\odot$. *Spitzer* IRS spectra of the star-forming BCG in Z3146 detect strong molecular hydrogen lines from warm H_2 with an estimated mass of $\sim 10^{10}$ $M_\odot$ (Egami et al. 2006a). This provides confirmation that the molecular gas masses can be very large in these BCGs.

We note that a correlation between integrated molecular gas mass and Hα luminosity in BCGs has been found by Edge (2001) and Salomé & Combes (2003). In Figures 7 and 8 we plot the molecular mass against our estimated IR luminosity and SFR (listed in Table 2). As found in normal star-forming galaxies (e.g., Young et al. 1986; Kennicutt 1998), we see a correlation between measured molecular gas mass and both the IR luminosity and the SFR in the BCGs. The ratio of molecular gas mass to SFR gives a gas depletion timescale which is roughly 1 Gyr. The gas depletion timescale is roughly constant over a range of 2 orders of magnitude in molecular gas mass and SFR. Our value of $\sim$1 Gyr is in good agreement with the mean value of $\sim$2 Gyr found in normal star-forming galaxies by Young et al. (1986), which have molecular gas masses in the range $\sim 10^9$–10^{10} $M_\odot$. The long lifetime of the molecular gas in these BCGs is in contrast to the much shorter cooling times for the gas over a range of temperatures. The hotter phases cool in times of $\sim 10^6$–10^8 yr (Peterson & Fabian 2006), while the molecular gas cools on even shorter timescales (e.g., Jaffe et al. 2001). Given that clusters are relatively young (perhaps 4–6 Gyr since the last major merger),

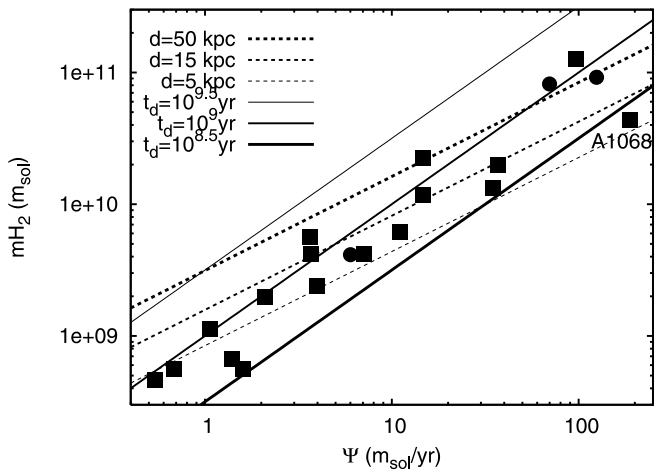

FIG. 8.—Correlation of H_2 mass from CO luminosity and SFR. Two BCGs, A1835 and Z3146, discussed by Egami et al. (2006a), are shown as circles in the top right portion of the figure. The dotted lines are taken from eq. [4] of Kennicutt (1998) using different values for the diameter of the star-forming region. The diameter of the star-forming region tends to be larger for more luminous objects. Solid lines are computed assuming gas depletion timescales of $10^{8.5}$, 10^9, and $10^{9.5}$ yr. See the legend at the upper left.

it is possible that there may have been insufficient time for a complete steady state (cooling leads to cold gas leads to star formation) to be set up.

7.1. *The Size Scale of Star Formation and Its Relation to the Optical Emission-Line Nebulae*

In nearby galaxies there is an empirical relation between SFR per unit area and molecular gas surface density. This relation can be described in terms of a Schmidt-Kennicutt law (Kennicutt 1998),

$$\left(\frac{\dot{\Sigma}_{\rm SFR}}{M_\odot\ {\rm yr}^{-1}\ {\rm kpc}^{-2}}\right) = 2.5\times10^{-4}\left(\frac{\Sigma_{\rm gas}}{M_\odot\ {\rm pc}^{-2}}\right)^{1.4}, \quad (4)$$

where $\Sigma_{\rm gas}$ is the surface density of molecular and atomic gas and $\dot{\Sigma}_{\rm SFR}$ is the SFR per unit area. We can use this relation to estimate the size scale of the star-forming region. We make the assumption that the star formation is distributed in a region of area $d^2_{\rm kpc}$, where $d_{\rm kpc}$ is a diameter in kpc, and the surface density $\Sigma_{\rm gas} = M_{\rm H_2}/d^2_{\rm kpc}$, where $M_{\rm H_2}$ is the molecular gas mass. Applying this to equation (4), we find a relation between molecular mass and SFR,

$$\left(\frac{M_{\rm H_2}}{M_\odot}\right) = 3.7\times10^8 d^{0.57}_{\rm kpc}\left(\frac{\rm SFR}{M_\odot\ {\rm yr}^{-1}}\right)^{0.71}. \quad (5)$$

We have shown this line in Figure 8 computed for diameters $d_{\rm kpc} = 5$, 15, and 50. We see that the data are consistent with a Schmidt-Kennicutt law, but the diameter of the star-forming region is not well constrained. The diameter of the star-forming region tends to be larger for more luminous objects, as expected if the diameter is proportional to $L_{\rm X}/\dot{M}_{\rm X}$. Previous studies have shown that the Schmidt law predicts the SFRs within a factor of a few for galaxies over a wide range of morphologies and SFRs, including starburst galaxies (Kennicutt 1998). The previous study of two BCGs by McNamara et al. (2006) suggested that the star formation law holds even in BCGs. However, Figure 7 shows that at high molecular gas masses $M_{\rm H_2} > 10^{10}\ M_\odot$, some BCGs show inferred diameters $\gtrsim$50 kpc, which are much larger than suggested by the sizes of the emission-line nebulae.

The sources with the largest estimated star formation regions are R1532+30, A1664, and Z8197, with estimated star formation region size scales of 70, 50, and 30 kpc, respectively, estimated using the Schmidt-type star formation law. None of these is well resolved, and all have FWHMs near the diffraction limit of 7″ at 24 μm. For R1532+30 at $z = 0.36$, the FWHM corresponds to a size of 35 kpc. This is below the estimated size of the star-forming region, $R \sim 70$ kpc. Likewise, for A1664 and Z8197, with redshifts of 0.128 and 0.114, the FWHM corresponds to about 15 kpc, and again this exceeds the estimated size scale by a factor of 2–3. The size scale estimates using the star formation law are probably a factor of 2–3 too large for these objects. Those with the smallest estimated star formation regions are A85, A262, A2052, and NGC 4325, with estimated regions of smaller than 5 kpc. At redshifts of 0.0551, 0.0166, 0.0351, and 0.0259, 7″ (diffraction limit at 24 μm) corresponds to 7, 2.3, 5, and 3.6 kpc, respectively. The objects with the smallest estimated regions are the nearest and so can be resolved in the IRAC images. For A85, the star-forming region could be the unresolved source at 8 μm that is southeast of the BCG nucleus. The BCG is resolved at 8 μm. For A262 and NGC 4235, the BCG is the source of the 24 μm emission and is resolved at both 24 and 8 μm, consistent with the estimate for the star-forming region size of a few kpc. For A2052, the BCG also hosts star formation in its nucleus. The emission is unresolved at 24 μm but resolved at 8 μm. This is consistent with the estimated size of the star-forming region of a few kpc. Except for the case of A85, the estimated sizes of the star-forming regions of a few kpc are consistent with the sizes estimated from the images. In summary, the Kennicutt-Schmidt law gives sizes which are generally consistent with those estimated from the images for the small and average sizes, although the largest sizes seem to be too large by factors of 2–3.

We note that the emission-line nebulae in cool cores tend to have a bright central region with a diameter of order 10 kpc (e.g., Heckman et al. 1989), with fainter gas extending to larger scales (e.g., Jaffe et al. 2005), which is comparable to the inferred size of the star formation region. Observations of extended H I absorption in the emission-line nebula of A2597 suggest that the optical nebulae are photon-bounded and are the ionized skins of cold atomic and molecular clouds (O'Dea et al. 1994). In addition, molecular hydrogen has been found to be associated with emission-line filaments in some BCGs (e.g., Donahue et al. 2000; Edge et al. 2002; Hatch et al. 2005; Jaffe et al. 2005; Egami et al. 2006a; Johnstone et al. 2007). Interferometric CO observations show molecular gas associated with the emission-line nebula in A1795 (e.g., Salomé & Combes 2004). Also, *HST* far-UV (FUV) images show FUV continuum from young stars associated with the emission-line nebulae in A1795 and A2597 (O'Dea et al. 2004). Thus, the spatial association of the FUV, the CO, the H_2, and the optical emission-line nebulae suggest that star formation occurs in molecular gas which lies in the optical emission-line nebulae.

Our estimated size scale of $d \sim 15$ kpc for the star formation region could be biased. Objects that have larger and more diffuse star formation regions would have had larger molecular gas masses and so would have been detected. Similarly, BCGs with lower and more concentrated star formation regions might have been missed.

8. THE CONNECTION BETWEEN STAR FORMATION AND THE PROPERTIES OF THE HOT ICM

We used archival *Chandra* and *XMM-Newton* observations to calculate X-ray inferred mass deposition rates and cooling times for 14 of the selected clusters. We required at least 15,000 counts from the source in each observation to generate reliable deprojected spectra. This restricted the cluster sample to 11 with suitable *Chandra* archive data and 3 with *XMM-Newton* archive data (R0338+09, R2129+00, and A115).

The *Chandra* data were analyzed using CIAO, version 4.0 beta 2, with CALDB, version 3.4.1, provided by the *Chandra* X-ray Center (CXC). The level 1 event files were reprocessed to apply the latest gain and charge transfer inefficiency correction and filtered for bad grades. Where available, the improved background screening provided by VFAINT mode was applied. The background light curves of the resulting level 2 event files were then filtered for periods affected by flares. For the nearer clusters ($z < 0.3$), background spectra were extracted from blank-sky background data sets available from the CXC and cleaned in the same way as the source observations. The normalizations of these cleaned background files were scaled to the count rate of the source observations in the 9–12 keV band. For more distant clusters, background spectra were extracted from suitable, source-free regions of the source data sets.

The *XMM-Newton* MOS data were reprocessed using the `emchain` task from *XMM-Newton* SAS, version 7.1.0, to generate calibrated event files from the raw data. Cosmic-ray filtering

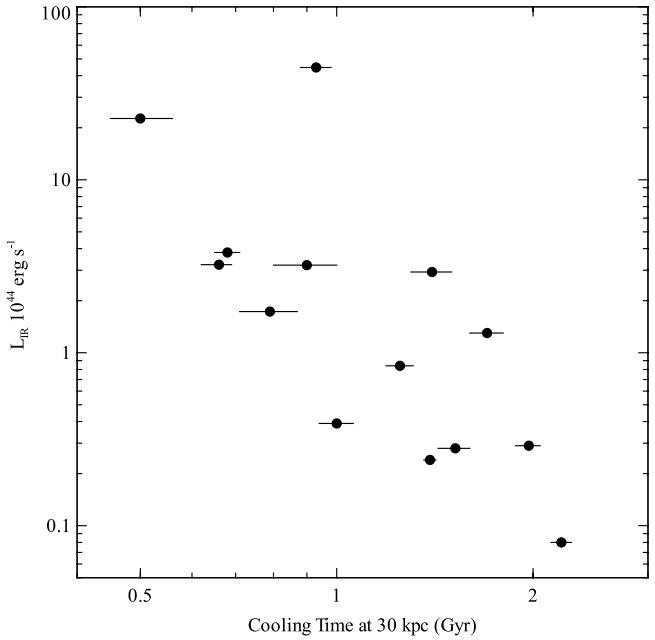

FIG. 9.—IR luminosity vs. X-ray-derived cooling times at a radius of 30 kpc. BCGs have higher IR luminosity in clusters with shorter cooling times.

TABLE 4
MASS DEPOSITION RATES

Cluster	$\dot{M}_S$ ($M_\odot$ yr^{-1})	$\dot{M}_I$ ($M_\odot$ yr^{-1})
A1068	30^{+20}_{-10}	440^{+10}_{-10}
R1532+30	400^{+200}_{-200}	1900^{+100}_{-100}
PKS 0745−1	200^{+40}_{-30}	1080^{+50}_{-40}
A1664	60^{+20}_{-20}	330^{+20}_{-20}
R0338+09	17^{+5}_{-3}	270^{+6}_{-6}
A2204	70^{+40}_{-40}	860^{+60}_{-60}
A115	6^{+11}_{-6}	190^{+10}_{-10}
R2129+00	6^{+30}_{-6}	380^{+30}_{-20}
A1204	50^{+40}_{-30}	620^{+30}_{-30}
A3112	10^{+7}_{-5}	220^{+10}_{-10}
A4059	5^{+2}_{-1}	105^{+2}_{-3}
A0085	6^{+8}_{-4}	210^{+10}_{-10}
A2052	5^{+1}_{-1}	72^{+1}_{-1}
A0262	$1.8^{+0.4}_{-0.2}$	10^{+1}_{-1}

NOTES.—Mass deposition rates calculated within $r_{\rm cool}$ using *Chandra* and *XMM-Newton* data. $\dot{M}_S$ is a measure of the mass deposition rate consistent with the X-ray spectra, and $\dot{M}_I$ is a measure of the mass deposition rate if heating is absent. Sources are listed in order of decreasing SFR.

was applied by selecting only PATTERNs 0–12, and bright pixels and hot columns were removed by setting FLAG = 0. Soft proton flares were removed by generating a light curve for photons of energy >10 keV, where the emission is dominated by the particle-induced background, and rejecting high background periods. Blank-sky background spectra were produced using the blank-sky background event files available from the *XMM-Newton* Science Operations Center and calibrated according to Read & Ponman (2003).

Spectra were extracted in concentric annuli centered on the X-ray surface brightness peak with a minimum of 3000 counts in each annulus. *Chandra* spectra were analyzed in the energy range 0.5–7.0 keV and *XMM-Newton* spectra in the range 0.3–10 keV. Suitable response files (ARFs and RMFs) were calculated and grouped together with the source spectrum, binned with a minimum of 30 counts.

Deprojected temperature and density profiles were calculated using a direct spectral deprojection method (Sanders & Fabian 2007; H. R. Russell et al., in preparation), which creates "deprojected spectra" using a model-independent approach, assuming only spherical geometry. Instead of correcting for projection by combining a series of models, this new method subtracts the projected spectra from each successive annulus to produce a set of deprojected spectra.

The resulting deprojected spectra were analyzed in XSPEC, version 11.3.2 (Arnaud 1996). Gas temperatures and densities were found by fitting each spectrum with an absorbed single-temperature plasma model [`phabs(mekal)`]. The redshift was fixed to the value given in Table 1 of Paper I, and the absorbing column density was fixed to the Galactic values given by Kalberla et al. (2005). The temperature, abundance, and model normalization were allowed to vary. We used the deprojected temperature and density to determine the cooling time of the gas at each radius. The cooling radius was defined to be the radius within which the gas has a cooling time less than 7.7×10^9 yr, corresponding to the time since $z = 1$.

In Figure 9 we plot the infrared luminosity versus the cooling time at a radius of 30 kpc. We see that BCGs with shorter cooling times have higher IR luminosities, consistent with the results of Egami et al. (2006b). This is consistent with the hypothesis that the clusters with shorter cooling times have higher SFRs, which result in higher IR luminosity.

We calculate two different measures of the mass deposition rate. A maximum mass deposition rate, $\dot{M}_I$, is calculated from

$$\dot{M}_I = \frac{2\mu m_{\rm H}}{5k_{\rm B}} \frac{L(<r_{\rm cool})}{T(r_{\rm cool})}, \quad (6)$$

where $\mu m_{\rm H}$ is the mean gas mass per particle and the luminosity was determined over the energy range 0.01–50 keV. Here $L(<r_{\rm cool})$ is directly proportional to the energy required to offset the cooling, and $\dot{M}_I$ is a measure of the mass deposition rate if heating is absent.

We calculate $\dot{M}_S$ by repeating the spectral fitting to the annuli within the cooling radius but now adding a cooling flow model (`mkcflow`) to the absorbed single-temperature model [`phabs(mekal+mkcflow)`]. The XSPEC model `mkcflow` models gas cooling between two temperatures and gives the normalization as a mass deposition rate, $\dot{M}_S$. For each spectrum, the temperature of the `mekal` component was tied to the high temperature of the `mkcflow` component, and the abundances of the two components were tied together. The low temperature of the cooling flow model was fixed to 0.1 keV. Here $\dot{M}_S$ is a measure of the maximum rate (upper limit) that gas can be cooling below X-ray temperatures and be consistent with the X-ray spectra. Detailed spectra of nearby bright clusters (Peterson et al. 2003; Fabian et al. 2006) tend to show an absence of the X-ray-coolest gas and indeed for the inferred $\dot{M}$ to be a function of temperature within a cluster. Better quality data for the objects here may lead in some cases to lower estimates of $\dot{M}_S$. We have listed the mass deposition rates for each cluster in Table 4 and plotted these values against SFRs estimated from the IR luminosity in Figure 10.

8.1. *Implications*

We see that the SFR is proportional to (but significantly less than) the two estimates of mass accretion rate. The results show that the SFR is about 30–100 times smaller than $\dot{M}_I$ and 3–10 times

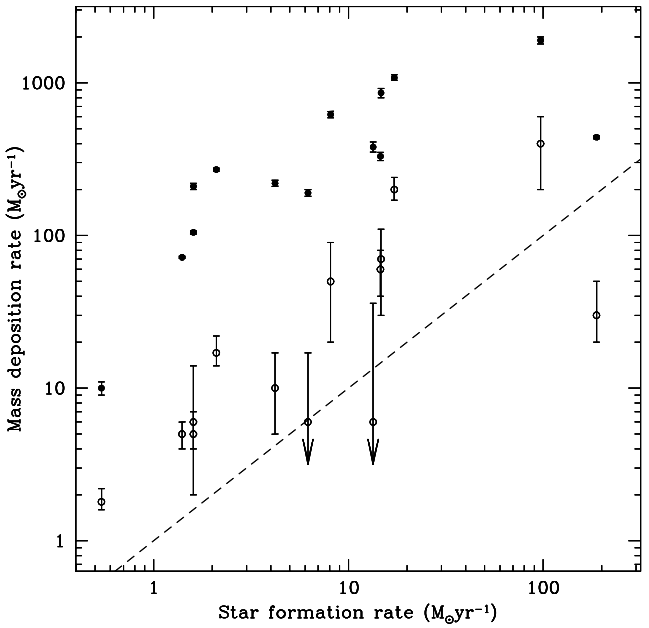

FIG. 10.—X-ray-derived mass deposition rate upper limits vs. estimated SFRs. The filled circles correspond to maximum mass deposition rates, $\dot{M}_I$, if heating is absent, and the open circles refer to $\dot{M}_S$, the mass deposition rate consistent with the X-ray spectra. The dashed line indicates equal star formation and mass deposition rates.

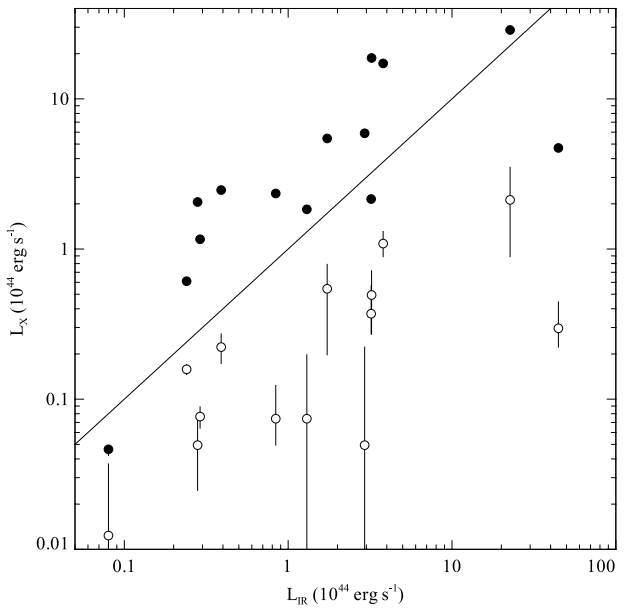

FIG. 11.—X-ray luminosity emitted with the cooling radius (a fiducial radius where the radiative cooling time is 7.7 Gyr, corresponding to a redshift of 1) is shown by filled circles vs. the *Spitzer* IR luminosity. The expected (missing) luminosity emitted below 1 keV by a continuous cooling flow operating from the cluster virial temperature to 0 K is shown by the open circles. If mixing with dusty cold gas causes the rapid nonradiative cooling of the intracluster gas below 1 keV, then this luminosity could emerge in the mid-IR.

smaller than $\dot{M}_S$. The observed trends between cooling time and IR luminosity and between $\dot{M}_S$ and the IR SFRs are consistent with the hypothesis that the cooling ICM is the source of the gas which is forming stars. Using a nearly identical approach to the X-ray analysis, Rafferty et al. (2006) found a similar trend using optical-UV SFRs. Star formation in these systems is generally not heavily obscured, and the SFRs are approaching and in some cases agree with the cooling upper limits, $\dot{M}_S$. This is consistent with the results from X-ray spectroscopy (e.g., Kaastra et al. 2001; Tamura et al. 2001; Peterson et al. 2001, 2003; Peterson & Fabian 2006), which suggests that most of the gas with a short cooling time at a few keV does not cool further. Sensitive, high-resolution X-ray spectroscopy should soon detect the cooling at the level of star formation in the Fe XVII lines if this picture is correct (e.g., Sanders et al. 2008). Our fraction of gas which does cool is a mean number and could be affected by our Hα selection, but we believe the use of a complete X-ray sample will allow this effect to be quantified. Nevertheless, this number could provide a constraint on the efficiency of feedback models that prevent the bulk of the ICM from cooling. If star formation is the ultimate sink for the cooling gas, then the fraction of the few keV gas which does cool all the way down should be comparable to the ratio SFR/$\dot{M}_X$, which we find to be roughly a few percent. This fraction is comparable for all the clusters. This suggests that the reheating mechanism (whatever it is) is very effective over a range of size scales and operates nearly all the time (i.e., with a short duty cycle; see McNamara & Nulsen 2007; Peterson & Fabian 2006 for reviews).

8.2. *Alternative Energy Sources*

We have proceeded with the assumption that the IR emission is solely due to star formation. Here we examine whether there are reasonable alternative sources of energy for this emission. First, we consider the hot gas, since dust mixing with the gas can be heated and become a source of mid-IR radiation (Dwek 1986; Dwek et al. 1990). We then consider cosmic rays and other heat sources.

The hot gas is potentially a rich energy source which could heat the dust. A consequence of such heating is the energy loss from the gas, which means the gas will cool, perhaps even exacerbating the cooling flow problem. It offers a solution to the problem seen in the X-ray spectra of cool core clusters in which gas is observed to cool down to only about 1 keV but no lower (Peterson et al. 2001, 2003; Tamura et al. 2001). The temperature profiles in clusters mean that the coolest gas is at the smallest radii, so if there is *nonradiative* cooling of gas at those radii, for example, due to mixing with cold dusty gas, X-ray spectra of the whole core would imply a cooling flow going down to just 1 keV and appearing to stop, more or less as observed. This can be seen as "the missing soft X-ray luminosity" problem (Fabian et al. 2002). What is meant by missing soft X-ray luminosity is the emission missing from a complete cooling flow when it appears from X-ray spectra to stop at, e.g., 1 keV.

Figure 11 shows the missing soft X-ray luminosity for our objects plotted against the IR luminosity as open circles. This was obtained by fitting the spectra with a cooling flow model which has a lower temperature limit of 1 keV. The missing soft X-ray luminosity is then the rate of energy release as that gas cools further to 0 K in some nonradiative manner. There is a correlation, but the normalization misses by about a factor of 5. This means that on average there is 5 times more L_{IR} than needed to account for nonradiative cooling of the gas below 1 keV.

Better agreement can be obtained by increasing the lower fitted temperature above 1 keV, but in that case the mass cooling rates rise from the more modest rates comparable to $\dot{M}_S$ in Figure 10 to the higher, pre-*XMM-Newton*/*Chandra* values of $\dot{M}_I$. This is just because L_{IR} is similar to L_{cool}, the luminosity of the cooling region in the core (i.e., where the radiative cooling time is less than, e.g., 5 Gyr), which is shown by the filled circles in Figure 11.

The result is that if dust mixing in hot gas is the only source of IR emission, then we have to face cooling rates much higher than

can be accommodated in terms of the observed molecular gas (Edge 2001) or observed SFRs (Table 3). More plausibly, hot gas mixing with dusty cold gas is the source of 10%–20% of the IR emission. In this case our results allow for modest mass cooling rates of up to tens to hundreds of $M_\odot$ yr^{-1}, comparable to the range shown in Table 3.

Cosmic rays also fail as an energy source, unless they are recycled. Since $L_{\rm IR} \sim L_{\rm cool}$ (to within about a factor of 3; see Fig. 11), the energy required for the IR is comparable with the thermal energy within $r_{\rm cool}$. Consequently, the cosmic-ray pressure would need to be high, with a pressure $P_{\rm CR} = f_{\rm CR} P_{\rm Th}$ with $f_{\rm CR} > 0.3$ and thermal pressure $P_{\rm Th}$. This is contrary to the quasi-hydrostatic appearance of the ICM in cluster cores.

Only if there is some efficient mechanism for energy to flow from the central accretion flow/AGN to the dust can an alternative be viable. In the absence of any such mechanism, we conclude that the UV radiation from massive star formation must be the energy source for the mid-IR emission measured by *Spitzer*.

9. SUMMARY

Paper I obtained *Spitzer* photometry of a sample of 62 BCGs in X-ray-bright clusters selected on the basis of BCG Hα flux, which tends to favor cool core clusters. They showed that at least half of the BCGs exhibit an IR excess with a luminosity $L_{\rm IR} \sim 10^{43}$–few $\times 10^{45}$ erg s^{-1}. In this paper we examined correlations in the data and discussed implications for cool core clusters.

BCGs with an IR excess are found mainly in clusters at high X-ray luminosity ($L_{\rm X} > 10^{44}$ erg s^{-1}). But not all high-$L_{\rm X}$ clusters have a BCG with an IR excess.

The IR luminosity is proportional to the Hα luminosity, suggesting that they are powered by the same or a related source of energy. We suggest that star formation is the dominant power source for the IR and Hα emission. The Hα luminosity falls below the Kennicutt (1998) relation probably because the spectroscopic apertures exclude much of the extended emission-line nebulae. The inferred star formation rates (SFRs) estimated from the IR luminosity are in the range of about 1–50 $M_\odot$ yr^{-1}. In most BCGs, supernovae produced by star formation with this SFR cannot account for the X-ray luminosity and so cannot be responsible for reheating the ICM.

The radio emission in the BCG is dominated by that produced by an AGN rather than star formation. However, there is a modest correlation between radio and IR emission. This suggests the feeding of the AGN and the fueling of the star formation may have a common origin, perhaps gas cooling from the hot ICM.

The mass of molecular gas (estimated from CO observations) is correlated with the IR luminosity as found for normal star-forming galaxies. The gas depletion timescale is about 1 Gyr. Given that clusters are relatively young (perhaps 4–6 Gyr since the last major merger), it is possible that there may have been insufficient time for a complete steady state (cooling leads to cold gas leads to star formation) to be set up.

We fit a Schmidt-Kennicutt relation to the molecular gas mass versus SFR and estimate a rough star-forming region diameter. For most BCGs the implied sizes of 10–20 kpc are comparable to those of the color variations seen in the IRAC data and to the optical emission-line nebulae. This is consistent with the hypothesis that star formation occurs in molecular gas associated with the emission-line nebulae and with evidence that the emission-line nebulae are mainly powered by ongoing star formation.

BCGs in clusters with shorter cooling times for the hot ICM have higher IR luminosities. We find a strong correlation between mass deposition rates ($\dot{M}_{\rm X}$) estimated from the X-ray emission and the SFR. The SFR is about 30–100 times smaller than $\dot{M}_I$, the mass accretion rate derived from imaging, and 3–10 times smaller than $\dot{M}_S$, the rate derived from spectroscopy. The observed trends between cooling time and IR luminosity and between $\dot{M}_S$ and the IR SFRs are consistent with the hypothesis that the cooling ICM is the source of the gas which is forming stars. The correlation between mass deposition rates estimated from the X-ray radiative losses and the SFRs suggests that the fraction of gas that does cool is set by the balance of heating and cooling by the cooling flow. The low value of SFR/$\dot{M}_{\rm X}$ suggests that heating is likely to be very efficient in preventing most of the gas at temperatures of a few keV from cooling further.

This work is based in part on observations made with the *Spitzer Space Telescope*, which is operated by the Jet Propulsion Laboratory, California Institute of Technology, under a contract with NASA. Support for this work at the University of Rochester and Rochester Institute of Technology was provided by NASA through an award issued by JPL/Caltech. We are grateful to the referee for helpful comments.

REFERENCES

Allen, S. W. 1995, MNRAS, 276, 947
Arnaud, K. 1996, in ASP Conf. Ser. 101, Astronomical Data Analysis Software and Systems V, ed. G. H. Jacoby & J. Barnes (San Francisco: ASP), 17
Baum, S. A., Heckman, T. M., Bridle, A., van Breugel, W. J. M., & Miley, G. K. 1988, ApJS, 68, 643
Baum, S. A., & O'Dea, C. P. 1991, MNRAS, 250, 737
Bell, E. F. 2003, ApJ, 586, 794
Best, P. N., von der Linden, A., Kauffmann, G., Heckman, T. M., & Kaiser, C. R. 2007, MNRAS, 379, 894
Birzan, L., Rafferty, D. A., McNamara, B. R., Wise, M. W., & Nulsen, P. E. J. 2004, ApJ, 607, 800
Blanton, E. L., Sarazin, C. L., & McNamara, B. R. 2003, ApJ, 585, 227
Böhringer, H., Matsushita, K., Churazov, E., Ikebe, Y., & Chen, Y. 2002, A&A, 382, 804
Calzetti, D. 2008, Nuovo Cimento, in press (arXiv: 0801.2558)
Cardiel, N., Gorgas, J., & Aragon-Salamanca, A. 1998, Ap&SS, 263, 83
Cowie, L. L., & Binney, J. 1977, ApJ, 215, 723
Cowie, L. L., Hu, E. M., Jenkins, E. B., & York, D. G. 1983, ApJ, 272, 29
Crawford, C. S., Allen, S. W., Ebeling, H., Edge, A. C., & Fabian, A. C. 1999, MNRAS, 306, 857
Crawford, C. S., & Fabian, A. C. 1992, MNRAS, 259, 265
———. 1993, MNRAS, 265, 431
Donahue, M., Mack, J., Voit, G. M., Sparks, W., Elston, R., & Maloney, P. R. 2000, ApJ, 545, 670
Donahue, M., Stocke, J. T., & Gioia, I. 1992, ApJ, 385, 49
Donahue, M., Sun, M., O'Dea, C. P., Voit, G. M., & Cavagnolo, K. W. 2007a, AJ, 134, 14
Donahue, M., & Voit, G. M. 1993, ApJ, 414, L17
Donahue, M., et al. 2007b, ApJ, 670, 231
Dunn, R. J. H., & Fabian, A. C. 2006, MNRAS, 373, 959
Dunn, R. J. H., Fabian, A. C., & Taylor, G. B. 2005, MNRAS, 364, 1343
Dwek, E. 1986, ApJ, 302, 363
Dwek, E., Rephaeli, Y., & Mather, J. C. 1990, ApJ, 350, 104
Edge, A. C. 2001, MNRAS, 328, 762
Edge, A. C., Stewart, G. C., & Fabian, A. C. 1992, MNRAS, 258, 177
Edge, A. C., Wilman, R. J., Johnstone, R. M., Crawford, C. S., Fabian, A. C., & Allen, S. W. 2002, MNRAS, 337, 49
Edwards, L. O. V., Hudson, M. J., Balogh, M. L., & Smith, R. J. 2007, MNRAS, 379, 100
Egami, E., Rieke, G. H., Fadda, D., & Hines, D. C. 2006a, ApJ, 652, L21
Egami, E., et al. 2006b, ApJ, 647, 922
Fabian, A. C. 1994, ARA&A, 32, 277
Fabian, A. C., Johnstone, R. M., & Daines, S. J. 1994, MNRAS, 271, 737
Fabian, A. C., & Nulsen, P. E. J. 1977, MNRAS, 180, 479

Fabian, A. C., et al. 2002, MNRAS, 335, L71
———. 2006, MNRAS, 366, 417
Hansen, L., Jorgensen, H. E., & Norgaard-Nielsen, H. U. 1995, A&A, 297, 13
Hansen, L., Jorgensen, H. E., Norgaard-Nielsen, H. U., Pedersen, K., Goudfrooij, P., & Linden-Vornle, M. J. D. 2000, A&A, 356, 83
Hatch, N. A., Crawford, C. S., & Fabian, A. C. 2007, MNRAS, 380, 33
Hatch, N. A., Crawford, C. S., Fabian, A. C., & Johnstone, R. M. 2005, MNRAS, 358, 765
Heckman, T. M. 1981, ApJ, 250, L59
Heckman, T. M., Baum, S. A., van Breugel, W. J. M., & McCarthy, P. 1989, ApJ, 338, 48
Hicks, A. K., & Mushotzky, R. 2005, ApJ, 635, L9
Hu, E. M. 1992, ApJ, 391, 608
Hutchings, J. B., & Balogh, M. L. 2000, AJ, 119, 1123
Jaffe, W., Bremer, M. N., & Baker, K. 2005, MNRAS, 360, 748
Jaffe, W., Bremer, M. N., & van der Werf, P. P. 2001, MNRAS, 324, 443
Johnstone, R. M., & Fabian, A. C. 1988, MNRAS, 233, 581
Johnstone, R. M., Fabian, A. C., & Nulsen, P. E. J. 1987, MNRAS, 224, 75
Johnstone, R., Hatch, N., Ferland, G., Fabian, A., Crawford, C., & Wilman, R. 2007, MNRAS, 382, 1246
Kaastra, J. S., Ferrigno, C., Tamura, T., Paerels, F. B. S., Peterson, J. R., & Mittaz, J. P. D. 2001, A&A, 365, L99
Kaiser, C. R., & Binney, J. 2003, MNRAS, 338, 837
Kalberla, P. M. W., Burton, W. B., Hartmann, D., Arnal, E. M., Bajaja, E., Morras, R., & Poppel, W. G. L. 2005, A&A, 440, 775
Kennicutt, R. C., Jr. 1998, ApJ, 498, 541
Koekemoer, A. M., O'Dea, C. P., Sarazin, C. L., McNamara, B. R., Donahue, M., Voit, G. M., Baum, S. A., & Gallimore, J. F. 1999, ApJ, 525, 621
Leitherer, C., et al. 1999, ApJS, 123, 3
McNamara, B. R. 1995, ApJ, 443, 77
———. 2004, in Proc. Riddle of Cooling Flows in Galaxies and Clusters of Galaxies, ed. T. Reiprich, J. Kempner, & N. Soker, http://www.astro.virginia.edu/coolflow/
McNamara, B. R., & Nulsen, P. E. J. 2007, ARA&A, 45, 117
McNamara, B. R., & O'Connell, R. W. 1989, AJ, 98, 2018
———. 1992, ApJ, 393, 579
———. 1993, AJ, 105, 417
McNamara, B. R., Wise, M. W., & Murray, S. S. 2004, ApJ, 601, 173
McNamara, B. R., et al. 2006, ApJ, 648, 164
Mittaz, J. P. D., et al. 2001, A&A, 365, L93
Narayan, R., & Medvedev, M. 2001, ApJ, 562, L129
O'Dea, C. P., Baum, S. A., & Gallimore, J. F. 1994, ApJ, 436, 669
O'Dea, C. P., Baum, S. A., Mack, J., Koekemoer, A. M., & Laor, A. 2004, ApJ, 612, 131
Oegerle, W. R., et al. 2001, ApJ, 560, 187
Omma, H., Binney, J., Bryan, G., & Slyz, A. 2004, MNRAS, 348, 1105
Peterson, J. R., & Fabian, A. C. 2006, Phys. Rep., 427, 1
Peterson, J. R., Kahn, S. M., Paerels, F. B. S., Kaastra, J. S., Tamura, T., Bleeker, J. A. M., Ferrigno, C., & Jernigan, J. G. 2003, ApJ, 590, 207
Peterson, J. R., et al. 2001, A&A, 365, L104
Quillen, A., et al. 2008, ApJS, 176, 39 (Paper I)
Rafferty, D. A., McNamara, B. R., Nulsen, P. E. J., & Wise, M. W. 2006, ApJ, 652, 216
Read, A. M., & Ponman, T. J. 2003, A&A, 409, 395
Romanishin, W. 1987, ApJ, 323, L113
Ruszkowski, M., & Begelman, M. 2002, ApJ, 581, 223
Salomé, P., & Combes, F. 2003, A&A, 412, 657
———. 2004, A&A, 415, L1
Sanders, J. S., & Fabian, A. C. 2007, MNRAS, 381, 1381
Sanders, J. S., Fabian, A. C., Allen, S. W., Morris, R. G., Graham, J., & Johnstone, R. M. 2008, MNRAS, 385, 1186
Smith, E. P., Bohlin, R. C., Bothum, G. D., O'Connell, R. W., Roberts, M. S., Neff, S. G., Smith, A. M., & Stecher, T. P. 1997, ApJ, 478, 516
Soker, N., Blanton, E. L., & Sarazin, C. L. 2002, ApJ, 573, 533
Sparks, W. B., Ford, H. C., & Kinney, A. L. 1993, ApJ, 413, 531
Sparks, W. B., Macchetto, F., & Golombek, D. 1989, ApJ, 345, 153
Tamura, T., et al. 2001, A&A, 365, L87
Tucker, W. H., & David, L. P. 1997, ApJ, 484, 602
Voigt, L. M., Schmidt, R. W., Fabian, A. C., Allen, S. W., & Johnstone, R. M. 2002, MNRAS, 335, L7
Voit, G. M., & Donahue, M. 1995, ApJ, 452, 164
———. 1997, ApJ, 486, 242
Wilman, R. J., Edge, A. C., & Swinbank, A. M. 2006, MNRAS, 371, 93
Young, J. S., Schloerb, F. P., Kenney, J. D., & Lord, S. D. 1986, ApJ, 304, 443
Yun, M. S., Reddy, N. A., & Condon, J. J. 2001, ApJ, 554, 803